JMEPEG (2011) 20:653–657
DOI: 10.1007/s11665-011-9917-0

1059-9495/$19.00

Characterization of Two Ti-Nb-Hf-Zr Alloys Under Different Cold Rolling Conditions

M. González, F.J. Gil, J.M. Manero, and J. Peña

(Submitted April 9, 2010; in revised form February 24, 2011)

The objective of this study is to obtain a new biomaterial to use in the load transfer medical implants field. The influence of cold work in the thermoelastic martensitic transformation and elastic modulus was investigated for a previously developed Ti-24.8Nb-16.2Hf-1Zr alloy (A1) and a new Ti-35Nb-9Hf-1Zr alloy (A2). The nanoindentation tests with spherical tip showed a decrease of the elastic modulus when increasing the cold work percentage. The lowest value (46 GPa) was achieved after the 95% reduction in thickness for A1. By contrast, the A2 alloy exhibits its lowest elastic modulus in the uncold-worked condition (58 GPa) and did not present evidences of thermoelastic martensitic transformation.

Keywords cold rolling, low elastic modulus, nanoindentation, Ni-free Ti alloys, shape memory effect

1. Introduction

Ideally, the elastic modulus of a biomaterial for load transfer implants has to be similar to that of cortical bone (~27 GPa) to avoid the stress shielding effect (Ref 1). Titanium alloys are useful for orthopedic implants due to their high corrosion resistance, high biocompatibility, and lower elastic modulus when compared to Cr-Co alloys and stainless steels.

On the other hand, NiTi alloys are commonly used shape memory metals in medical devices. Shape memory alloys have high damping capacity, high wear resistance, and low elastic modulus, which are interesting properties for orthopedic implants. However, the high concentrations of nickel generate nickel sensitivity problems (Ref 2, 3).

For this reason, many researches are specially focusing on β-type Ti alloys that exhibit low elastic modulus and possible thermoelastic martensitic transformation. Moreover, the high ductility of β-Ti alloys promotes a good coldworkability which permits to control the grain size to produce low modulus metals. Recently, it has been suggested that nano-size materials can be easily fabricated from metastable metals (Ref 4). In addition, it has been found that the elastic moduli of nanocrystalline materials are usually lower than the corresponding coarse-sized crystalline materials (Ref 5).

The objective of this study is to produce a new biomaterial for load transfer implants. For this purpose, the influence of cold work in the thermoelastic martensitic transformation and elastic modulus of the previously developed in our laboratories Ti-24.8Nb-16.2Hf-1Zr (wt.%) alloy (A1) and the new Ti-35Nb-9Hf-1Zr (wt%) alloy (A2) has been evaluated.

2. Experimental

A theoretical method based on molecular orbitals was used to predict the stable phase and design two Ti alloys (A1 and A2). This method also allows reducing time and cost of experimentation (Ref 6).

The method consists on the creation of a new map based on two quantum parameters, ($\overline{BO}$, $\overline{OE}$), calculated by the implementation of Khon-Sham of the Density Functional Theory (DFT) and based on a database of more than 140 alloys. $\overline{BO}$ represents the covalent bond strength between Ti and the alloying element and $\overline{OE}$ is correlated with the electronegativity and metallic radius of the element (Ref 6). The application of the resulting parameters to the data base permitted to build a new phase stability map. In the map two zones can be distinguished, delimited by the dot and dashed line, corresponding to the probability to obtain low elastic modulus and shape memory effect, respectively.

With this purpose, two pairs of quantum parameters ($\overline{BO}$, $\overline{OE}$) were selected from the β-zone, where the shape memory and low elastic modulus properties coexist (Fig. 1). Moreover, quantum parameters ($\overline{BO}$, $\overline{OE}$) for alloy A1 are near to the frontier between both properties, hence being more likely to produce a metastable phase and consequently thermoelastic martensite. The alloys chemical composition was then defined by choosing Nb, Hf, and Zr as alloying elements for their properties: β-stabilizers (Nb, Hf), higher mechanical strength (Hf), and biocompatibility (Nb, Hf, Zr). The resulting material compositions for the two alloys (A1 and A2) were Ti-24.8Nb-16.2Hf-1Zr (wt.%) and Ti-35Nb-9Hf-1Zr (wt.%), respectively.

This article is an invited paper selected from presentations at Shape Memory and Superelastic Technologies 2010, held May 16-20, 2010, in Pacific Grove, California, and has been expanded from the original presentation.

M. González, F.J. Gil, J.M. Manero, and **J. Peña**, Department of Materials Science and Metallurgy, Universitat Politècnica de Catalunya, Avda. Diagonal 647, 08028 Barcelona, Spain; and **J. Peña**, Materials Science, Elisava Escola Superior de Disseny, C/Ample 11-13, 08002 Barcelona, Spain. Contact e-mails: Marta.Gonzalez.Colominas@upc.edu, Francesc.Xavier.Gil@upc.edu, Jose.Maria.Manero@upc.edu, and jpenya@elisava.es.

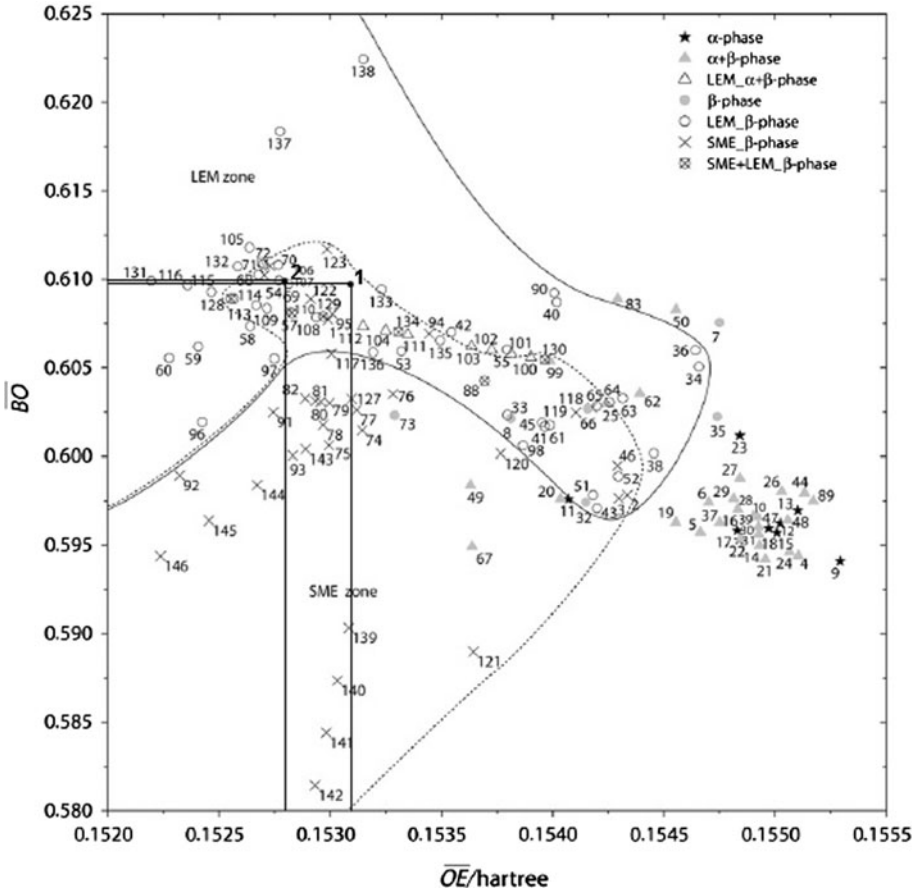

Fig. 1 Design map based on two quantum parameters, $\overline{BO}$ and $\overline{OE}$

Moreover, A2 alloy was designed to share three electronic magic numbers (*e*/*a* ratio of 4.24, Bo of 2.87 and Md of 2.45 eV) reported by Saito et al. as necessary to obtain a multifunctional alloy (Ref 7).

The determination of β-transus temperature (Ref 8) and Mo equivalent (Ref 9) was carried out using Eq 1 and 2, respectively, to design the heat treatment. The β-transus for pure Ti is reported as 882 °C and the addition of β-stabilizing solutes reduces this value.

$$T_{\beta\text{transusalloy}} = T_{\beta\text{transusTi}} - 7.22\%_{\text{wt}}\text{Nb} \quad \text{(Eq 1)}$$

$$[Mo]_{\text{eq}} = 0.28\%_{\text{wt}}Nb \quad \text{(Eq 2)}$$

The alloys were melted in 40 g bars from starting elements of 99.9% purity in an arc furnace in controlled Ar atmosphere. Samples of both alloys were quartz encapsulated for homogenization at 1100 °C for 12 h, heat treated at 1100 °C during 1.5 h and quenched in ice water at 0 °C. A Fischerscope x-ray System HDL equipment was used to verify the chemical composition of each alloy.

Samples of alloy A2 were cold rolled at low (5 and 10%) and high cold roll percentages (90, 95, and 99%) and samples of alloy A1 were also cold rolled at low (2, 3, and 5%) and high cold roll percentages (90 and 95%). The samples were cold rolled without lubrication using a rolling mill with a diameter of 55 mm at a rotating speed of 30 rpm at ambient temperature with a reduction of 5% per pass.

The different conditions were microstructurally characterized by Optical microscopy after Keller reactive attack (3 mL HCl, 2 mL HF, 5 mL HNO_3, and 190 mL H_2O) and by x-ray diffraction. Thin disks of 3 mm diameter were electropolished for transmission electron microscopy (TEM) in an electrolyte consisting of 400 mL butoxyethanol, 400 mL methanol, and 100 mL perchloric acid.

The elastic response for each condition was evaluated by instrumented nanoindentation using a spherical tip with a radius of 25 μm to evaluate the phase transformation induced by stress under indentation loading. The samples were mechanically polished and finished with colloidal silica to give a surface roughness with a $Ra < 100$ nm. Cyclic nanoindentation tests were conducted in a MTS Nano Indenter XP with Continuous Stiffness Measurement (CSM) module to a depth of 300 and 2000 nm. The tests were performed on rolled surfaces.

The reduced elastic modulus was calculated from spherical nanoindentation using the Hertz contact theory (Ref 10) in the elastic deformation range through Eq 3.

$$F = \frac{4}{3}E^{*}R^{1/2}h^{3/2} \quad \text{(Eq 3)}$$

where E^* is the reduced elastic modulus, R is the tip radius, and h is the indentation depth.

The elastic modulus was calculated from the reduced modulus using Eq 4.

$$\frac{1}{E^{*}} = \frac{1-\nu_{\text{m}}^2}{E_{\text{m}}} + \frac{1-\nu_{\text{i}}^2}{E_{\text{i}}} \quad \text{(Eq 4)}$$

where E^* is the reduced modulus, E_m, ν_m, and E_i, ν_i and are the elastic modulus and Poisson coefficient of the

material, and of the indenter material, diamond, respectively (Ref 11).

3. Results and Discussion

The higher Mo equivalent value corresponds to the A2 alloy with 9.8 compared to the 6.9 of A1 alloy. As it was expected the higher β-transus temperatures corresponded to the A1 alloy with 703 °C compared to the 629 °C of A2 alloy.

The microstructure of the untreated alloy A1 (0% C.W.) is composed mainly by a β-phase, together with a low fraction of α″. The alloy in the 5% C.W. condition (Fig. 2a) is mainly formed by stress-induced martensitic plates (α″) coming from cold-worked austenite. In the 90% C.W. condition it was not possible to observe the microstructure by optical microscopy because the plastic deformation induced by the higher cold-roll percentages refined coarse grains out of the detection limits.

However, β-prior grains were detected on the untreated and cold worked conditions of the alloy A2 (Fig. 2b). This is due to the fact that the β-phase is more stable because of the increment of β-stabilizer.

X-ray diffraction results confirmed the presence of β-phase in both alloys and also α″-phase in alloy A1. However, the A2 alloy did not present evidence of thermoelastic martensitic transformation induced by stress in the cold-worked samples (Fig. 3).

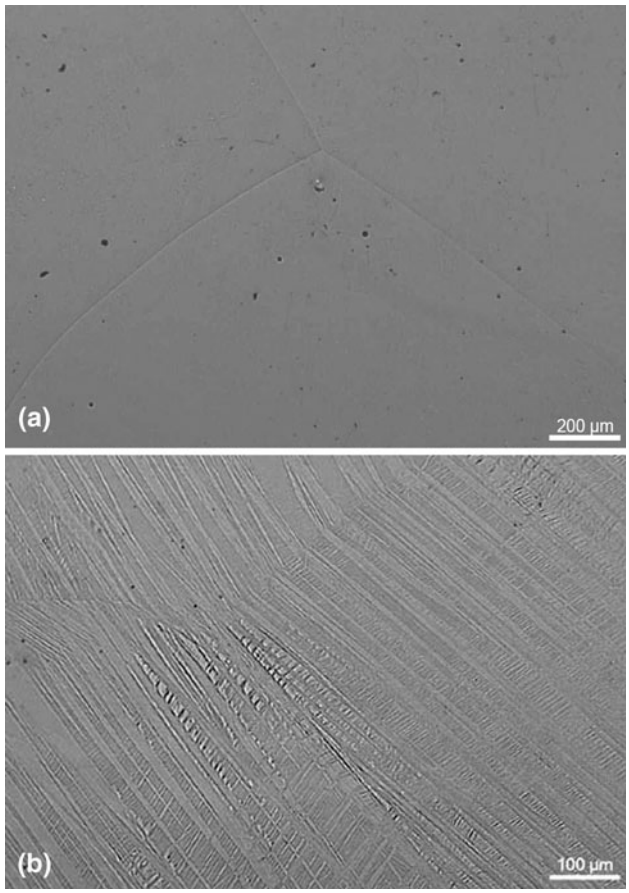

Fig. 2 Optical microscopy images of: (a) A1 alloy (5% C.W.) and (b) uncold-worked A2 alloy

More details about the microstructure of the high cold work conditions were observed by TEM. A nanocrystalline structure was observed from the 90% cold worked alloy A1. The typical electron diffraction pattern with continual diffraction rings confirmed the presence of many crystalline grains and the indexation of the rings corresponded to the reticular parameters of β-phase (Ref 12).

A bright-field image obtained by TEM from the 90% cold-rolled alloy A2 shows a dislocation network formed as a consequence of the plastic deformation (Fig. 3). In the selected area (Fig. 4), the electron diffraction pattern displays a distorted β-phase as a consequence of the deformation of the alloy.

The nanoindentation results associated with the alloy A1 showed that by increasing the cold rolling reduction from 0 to 95% a decrease in the elastic modulus from 65 to 46 GPa was observed (Fig. 5). The low elastic modulus of the alloy in the 95% C.W. condition is attributed to the nanocrystalline structure (Ref 12). However, it should be considered that nanoindentation, as surface test, is strongly dependent on the surface conditions and testing area (longitudinal or transversal) of the rolled specimens. Moreover, it gives localized modulus information.

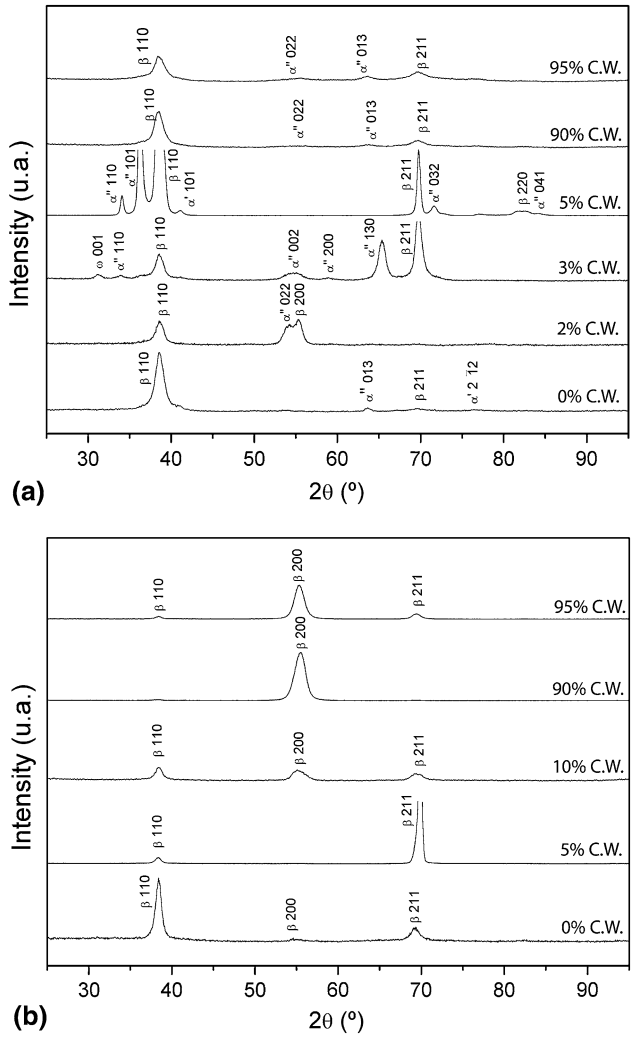

Fig. 3 X-ray diffraction patterns of: (a) alloy A1 after 2, 3, 5, 90, and 95% C.W. and (b) alloy A2 after 5, 10, 90, and 95% C.W

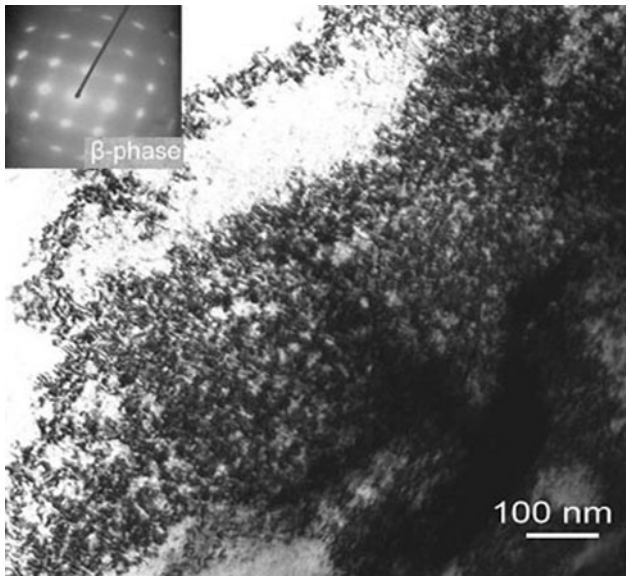

Fig. 4 Bright-field TEM image of the 90% cold worked alloy number 2 and electron diffraction pattern of the selected area

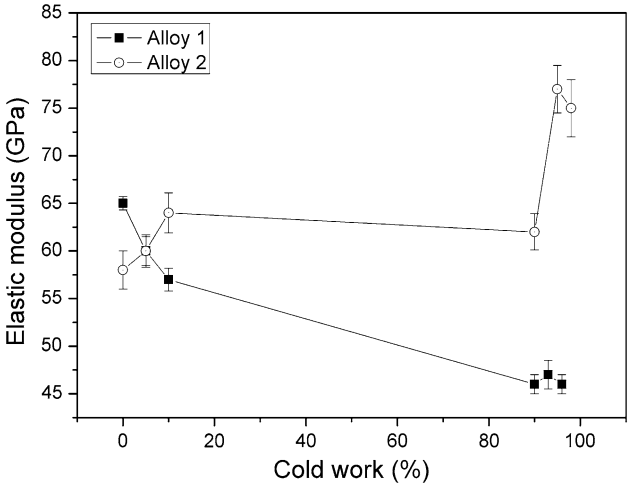

Fig. 5 Elastic modulus of the different cold work conditions of alloys A1 and A2 calculated by nanoindentation with a spherical tip

By contrast, elastic modulus values obtained for the alloy A2 augmented upon increase of the cold rolling reduction. This result could be explained because a nanocrystalline structure was not formed after the cold work treatment. It also could be explained because of the residual stresses of cold rolled samples. However, the untreated alloy A2 (0% C.W.) presented a very low elastic modulus of 58 GPa.

Load-displacement curve of A1 alloy evidenced a discontinuity on the loading portion reported as pop-in and hysteresis loops generated between the unloading and the re-loading curves (Ref 8). Both events are associated with the martensitic transformation. However, the A2 did not show changes on the loading curve and neither hysteresis loops, indicating that thermoelastic martensitic transformation did not take place in that alloy (Fig. 6a). On the other hand, as it was expected, A2 alloy neither presented traces of thermoelastic martensitic transformation in the cold-worked condition (Fig. 6b).

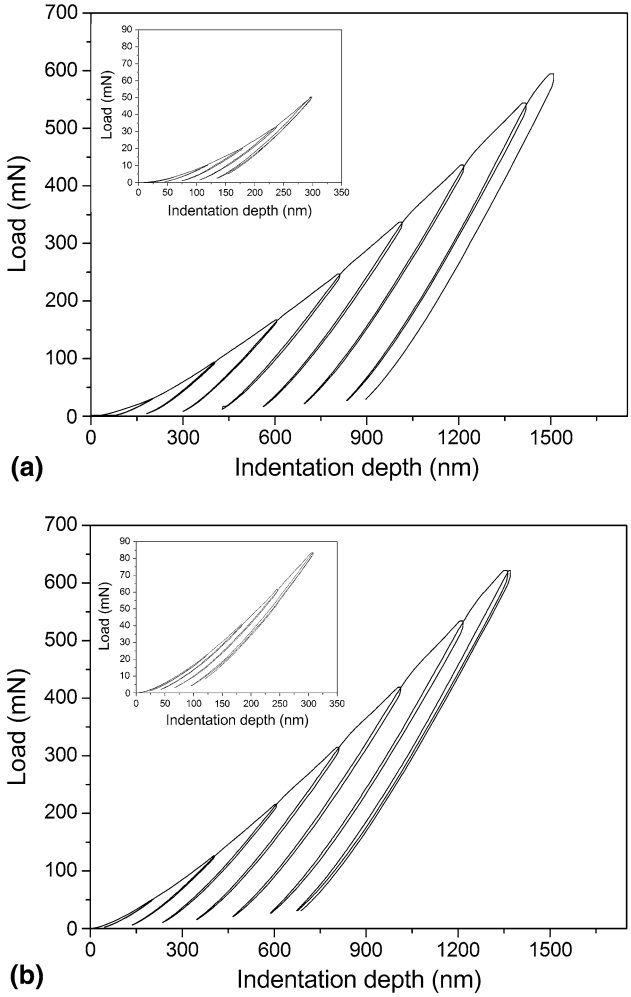

Fig. 6 Nanoindentation load-displacement curves: (a) of the uncold-worked A2 alloy and (b) with 95% reduction in thickness, obtained under cyclic increasing-load control conditions

4. Conclusions

Optical microscopy and x-ray diffraction results showed the presence of stress-induced martensite in the Ti-24.8Nb-16.2Hf-1Zr (A1) cold rolled alloy.

Moreover, the nanoindentation tests with spherical tip showed a decrease of the elastic modulus when increasing the cold work percentage. The lowest value (46 GPa) was achieved after the 95% reduction in thickness. The Ti-35Nb-9Hf-1Zr (A2) alloy did not present evidence of thermoelastic martensitic transformation and neither a decrease of the elastic modulus after cold rolling. However, it presents a low initial elastic modulus (58 GPa), compared with other alloys currently employed in the load transfer field. These results suggest that the three magic numbers are not the only parameters necessary to determine a multifunctional alloy with superelasticity, lower elastic modulus, high coldworkability, and dislocation-free plastic deformation mechanism, but also the Mo equivalent contents seems to be important to define such properties. Therefore, A2 does not present all such features because its Mo content is too high and avoid the transformation from β-phase to thermoleastic martensite.

In conclusion, these results show that both alloys A1 (95% C.W.) and the uncold-worked A2 exhibit low elastic modulus, which are about twice the ''ideal'' value of cortical human bone (27 GPa) and lower than those presented by the commercial alloys used as load transfer implant materials. Moreover, are therefore good candidates for load transfer implants, enhancing bone remodeling due to the reduction of the shielding effect.

Acknowledgments

This study was carried out with the support of the Generalitat de Catalunya Commission for the Universities and Research of the Department of Innovation, Universities and Companies and the European Social Fund.

References

1. M. Niinomi, Recent research and Development in Titanium Alloys for Biomedical Applications and Healthcare Goods, *Sci. Technol. Adv. Mater.*, 2003, **4**(5), p 445–454
2. E. Denkhaus and K. Salnikow, Nickel Essentiality Toxicity, and Carcinogenicity, *Crit. Rev. Oncol. Hematol.*, 2002, **42**(1), p 35–56
3. A. Michiardi, C. Aparicio, B.D. Ratnerb, J.A. Planell, and J. Gil, The Influence of Surface Energy on Competitive Protein Adsorption on Oxidized NiTi Surfaces, *Biomaterials*, 2006, **28**(4), p 586–594
4. Y.L. Hao, Titanium Alloy with Extra-Low Modulus and Superelasticity and its Producing Method and Processing Thereof US 2007/0137742 A1, 2007
5. J. Schiøtz, F.D. Di Tolla, and K.W. Jacobsen, Softening of Nanocrystalline Metals at Very Small Grain Sizes, *Nature*, 1998, **391**, p 561–563
6. M. Arciniegas, J. Peña, J.M. Manero, J.C. Paniagua, and F.J. Gil, Quantum Parameters for Guiding the Design of Ti Alloys with Shape Memory and/or Low Elastic Modulus, *Philos. Mag.*, 2008, **88**(17), p 2529–2548
7. T. Saito, T. Furuta, J.-H. Hwang, S. Kuramoto, K. Nishino, N. Suzuki, R. Chen, A. Yamada, K. Ito, Y. Seno, T. Nonaka, H. Ikehata, N. Nagasako, C. Iwamoto, Y. Ikuhara, and T. Sakuma, Multifunctional Alloys Obtained via a Dislocation-Free Plastic Deformation Mechanism, *Science*, 2003, **300**, p 464–467
8. M. González, J. Peña, J.M. Manero, M. Arciniegas, and F.J. Gil, Design and Characterization of New Ti-Nb-Hf Alloys, *J. Mater. Eng. Perform.*, 2009, **18**, p 490–495
9. R. Boyer, G. Welsch, and E.W. Collings, *Materials Properties Handbook: Titanium Alloys*, ASM International, Materials Park, 1998, p 5–11
10. G.M. Pharr, Measurement of Mechanical Properties by Ultra-Low Load Indentation, *Mater. Sci. Eng. A*, 1998, **253**(1–2), p 151–159
11. A.C. Fischer-Cripps, A Review of Analysis Methods for Sub-Micron Indentation Testing, *Vacuum*, 2000, **58**(4), p 569–585
12. M. González, J. Peña, J.M. Manero, M. Arciniegas, and F.J. Gil, Optimization of the Ti-16.2Hf-24.8Nb-1Zr Alloy by Cold Working, *J. Mater. Eng. Perform.*, 2009, **18**, p 506–510